

On the determination of Young's modulus of thin films with impulse excitation technique

M.F. Slim^{a)} and A. Alhussein^{b)}

ICD-LASMIS, Université de Technologie de Troyes, UMR 6281, CNRS, Antenne de Nogent, Pôle Technologique de Haute-Champagne, Nogent 52800, France; and Nogent International Center for CVD Innovation, LRC CEA-ICD-LASMIS, UTT, Antenne de Nogent-52, Pôle Technologique de Haute-Champagne, Nogent 52800, France

A. Billard

IRTES-LERMPS, UTBM, site de Montbéliard, Belfort cedex 90010, France; and LRC CEA-IRTES-LERMPS, UTBM, site de Montbéliard, Belfort cedex 90010, France

F. Sanchette

ICD-LASMIS, Université de Technologie de Troyes, UMR 6281, CNRS, Antenne de Nogent, Pôle Technologique de Haute-Champagne, Nogent 52800, France; and Nogent International Center for CVD Innovation, LRC CEA-ICD-LASMIS, UTT, Antenne de Nogent-52, Pôle Technologique de Haute-Champagne, Nogent 52800, France

M. François

ICD-LASMIS, Université de Technologie de Troyes, UMR 6281, CNRS, Antenne de Nogent, Pôle Technologique de Haute-Champagne, Nogent 52800, France

(Received 25 July 2016; accepted 3 November 2016)

The purpose of this paper is to propose a critical assessment of Young's modulus determination of coated materials using Impulse Excitation Technique (IET). In this technique, the coated substrate is excited by an impulse and the acoustic vibrations are recorded. The frequency of the first bending mode is then used in a mechanical model to obtain the Young's modulus of the coating. The existing models are based on two different theories: the flexural rigidity of a composite beam and the Classical Laminated Beam Theory (CLBT). The aim of the present paper is to assess the accuracy (trueness and precision) of the technique. For this, different models proposed in the literature are compared with a finite element model of the specimen for various conditions. The trueness and precision of models were evaluated and the best model was identified. Then a detailed uncertainty budget is performed to identify and quantify the most influent factors on the global uncertainty.

I. INTRODUCTION

Thin films are widely used in various applications to enhance the surface properties and characteristics of materials. They are used in biomedical, automotive, aeronautic, military, electronic, and energy domains.^{1–3} The physical properties of coatings often differ from those of bulk materials and depend essentially on the techniques of elaboration and their parameters.^{4,5} So to optimize the reliability and the performance of coated components, the physical, chemical, and mechanical properties of a coating must be controlled. In this paper the interest will be focused on the elastic modulus of thin films.

In the last two decades, many methods were developed to determine the elasticity constants of bulk and coated materials which can be classified into two groups: static and dynamic techniques.^{6,7} Among the dynamic techniques, we

can mention in particular the resonant ultrasound spectroscopy^{8–10} and the vibrational technique.^{6,11–14} In the following, more attention will be given to the determination of the coatings Young's modulus using the vibrational approach also known as the Impulse Excitation Technique (IET).

All the mathematical relations are based on the Euler–Bernoulli bending beam theory which does not take into account the effect of shear and rotatory inertia. To consider both effects, Pickett has simplified the Timoshenko's equation and determined some correction factors.¹⁵ Then these factors were improved by Spinner and Tefft^{16–19} who have determined the correcting factors as a function of different vibration modes and sample geometry. Their works have led to the birth of the ASTM-E1876 test method in 1999, updated in 2015.²⁰

The IET is a nondestructive technique, highly precise and easy to use to measure the elasticity constants of a wide range of materials: metals, composites, ceramics, coatings ... etc.^{7,11,13,21} These advantages qualify this technique to be adopted as another alternative to measure the Young's modulus of coatings. The first experience using a bilayer material (substrate + coating) was carried

Contributing Editor: Erik G. Herbert

Address all correspondence to these authors.

^{a)}e-mail: mohamedfaresslim@gmail.com, mohamed_fares.slim@utt.fr

^{b)}e-mail: akram.alhussein@utt.fr

DOI: 10.1557/jmr.2016.442

out by Berry.²² The test relies on the measurement of the sample resonance frequencies before and after deposition.

Many researchers have used the IET for various films elaborated differently with different thickness. By comparing four measurement methods, Bellan et al.⁶ have shown that IET gives good and accurate results. They have evaluated the elasticity modulus of SiC and PyC films elaborated by Chemical Vapor Deposition (CVD) with 35 μm and 95 μm of thickness, respectively. López-Puerto,¹² Peraud,²³ and Etienne²⁴ have measured the Young's modulus of various thin films, respectively: Au/Al, SiC/NiTi (2 μm obtained by dynamic ion mixing) and TiN (0.2 μm elaborated by ion implantation). All these authors have used different mathematical relations. The lack of information concerning the validity range of the models and the observed divergence between them, in the case of higher ratio of coating/substrate thickness, gives the motivation to do a thorough study on the models proposed in the literature. Also, a thorough study of error/uncertainty sources seems to be inexistent in the literature.

The goal of this paper is not only to review all the mathematical relations developed to determine the Young's modulus of coatings but also to investigate their advantages, limits and do an investigation on the measurement accuracy. Although the method applied here is very general, the quantitative description is based on experiments performed on aluminum films, as a concrete example. Firstly, we introduce the theoretical background of the IET and review the models. Secondly, we present the deposition conditions of the aluminum film and the followed experimental protocol to determine its Young's modulus. Then, we compare all the analytical expressions with the finite element model and studying the impact of the assumptions on the validity of each model. Finally, an uncertainty study is realized to identify the errors or uncertainty sources and evaluate their contributions.

II. MEASUREMENT PRINCIPLES

A. Theoretical background

Based on the Euler–Bernoulli beam theory which does not take into account the shear and rotary inertia effect, the motion of a beam subjected to flexural vibration can be described by the following equation²⁵:

$$\rho S \frac{\partial^2 U(x, t)}{\partial t^2} + \frac{\partial^2}{\partial x^2} \left(EI \frac{\partial^2 U(x, t)}{\partial x^2} \right) = 0 \quad (1)$$

This differential equation can be solved analytically and allows to determine the shapes and the frequencies of the vibration modes. The resonance frequencies can be determined from this following equation²⁵:

$$f_n = \frac{X_n^2}{l^2} \sqrt{\frac{EI}{\rho S}} \quad (2)$$

Where:

X_n : constant which depends on the boundary conditions applying to the beam (called also nondimensional eigenfrequencies).

In the present study, we used a free–free system for which:

$$X_n = (2n + 1) \frac{\pi}{2} \quad (3)$$

B. Homogeneous beam

The IET is not only used for beam specimen but can be used for any sample shape: rod, disc, and arbitrary geometry.^{20,26} In the case of a free–free beam with a rectangular cross-section, the Young's modulus can be determined by the following formula [Eq. (4)]²⁰:

$$E = k_1 f_s^2 \rho_s \frac{l^4}{h_s^2} T_f \quad (4)$$

Where:

$$k_1 \sim 0.9465 \quad .$$

Index s means the substrate.

T_f is the geometrical correction factor introduced to take into account the shear and rotatory effects.²⁰

$$T_f = 1 + 6.585(1 + 0.0752\nu + 0.8109\nu^2) \left(\frac{h_s}{l}\right)^2 - 0.868 \left(\frac{h_s}{l}\right)^4 - \left[\frac{8.34(1 + 0.2023\nu + 2.173\nu^2) \left(\frac{h_s}{l}\right)^4}{1 + 6.338(1 + 0.1408\nu + 1.536\nu^2) \left(\frac{h_s}{l}\right)^2} \right] \quad (5)$$

If $l/h_s \geq 20$, it can be simplified into the following expression:

$$T_f = 1 + k_2 (h_s/l)^2 \quad (6)$$

Where:

$$k_2 \sim 6.585 \quad .$$

C. Extension to coated substrates

The principle of the measurement is to perform a two-steps frequency measurement before and after deposition. Then knowing the elastic modulus of the substrate, the density of both substrate and coating and the resonance frequencies of the composite beam and the substrate, the Young's modulus of the film can be determined through analytical expressions. In the literature, all models, allowing

to determine the coating Young's modulus, are based on two different theories: the flexural rigidity of a composite beam and the classical laminated beam theory.

III. REVIEW OF THE MODELS PROPOSED IN THE LITERATURE

A. Models based on the flexural rigidity of a composite beam

During bending, a composite beam is loaded with a moment. The resistance to this moment (EI), also known as the flexural rigidity, of the entire composite beam can be expressed as the sum of the flexural rigidity of each material [Eq. (7)].²⁷ The coating is supposed to be perfectly homogeneous, compact, and adherent to the substrate.

$$E_t I_t = E_s I_s + E_c I_c \quad (7)$$

The indexes t, s, and c mean whole (homogenized) bilayer beam, substrate, and coating, respectively.

The density per unit of area of the composite beam can be determined by the following equation:

$$\rho_t S_t = \rho_s S_s + \rho_c S_c \quad (8)$$

By replacing EI by $E_t I_t$ and ρS by the effective density of the composite beam $\rho_t S_t$ in Eq. (2) we will obtain the resonance frequency of the composite beam:

$$f_t = \frac{X_n^2}{l^2} \sqrt{\frac{E_t I_t}{\rho_t S_t}} \quad (9)$$

1. Lopez's model

For a composite beam with a rectangular cross section, Lopez has developed an analytical expression to determine the film Young's modulus. The second moments of substrate and coating sections are respectively calculated as follows:

$$I_s = \frac{bh_s^3}{12} \quad (10)$$

$$I_c = \frac{bh_c h_s^2}{4} + \frac{bh_s h_c^2}{2} + \frac{bh_c^3}{3} \quad (11)$$

Replacing I_s and I_c by their correspondent expressions, in Eq. (9), leads to the frequencies ratio between the coated sample and the substrate.^{14,28}

$$(R_f)^2 = \frac{1 + R_E(3R_h + 6R_h^2 + 4R_h^3)}{1 + R_h R_p} \quad (12)$$

Where:

$$R_h = \frac{h_c}{h_s}$$

$$R_p = \frac{\rho_c}{\rho_s}$$

$$R_f = \frac{f_t}{f_s}$$

$$R_E = \frac{E_c}{E_s} \quad .$$

Then, the Young's modulus of the coating can be calculated as:

$$E_c = \frac{E_s}{3R_h + 6R_h^2 + 4R_h^3} \left[\left[(R_f)^2 (1 + R_h R_p) \right] - 1 \right] \quad (13)$$

This model does not consider the shift of the neutral axis after deposition. This simplification becomes increasingly inaccurate when the film thickness increases and for large R_E ratio.

2. Pautrot's model

The difference between Lopez's model and Pautrot's model is that the latter takes into account the shift of the neutral axis after deposition (Fig. 1). This shift can be determined by the equation which establishes the equilibrium of forces.²⁷

$$\int_{-h_s+e}^e \sigma_s dS + \int_e^{e+h_c} \sigma_c dS = 0 \quad (14)$$

$$e = \frac{E_s h_s^2 - E_c h_c^2}{2E_s h_s + 2E_c h_c} \quad (15)$$

$$I_s = \frac{bh_s^3}{12} + bh_s \left(\frac{h_s}{2} - e \right)^2 \quad (16)$$

$$I_c = \frac{bh_c^3}{12} + bh_c \left(e + \frac{h_c}{2} \right)^2 \quad (17)$$

Taking into consideration the shift of the neutral axis (e) in the expressions of second moments of both substrate and coating and replacing them in Eq. (9) lead to obtain the frequencies ratio between the coated sample and the substrate.^{11,14,28}

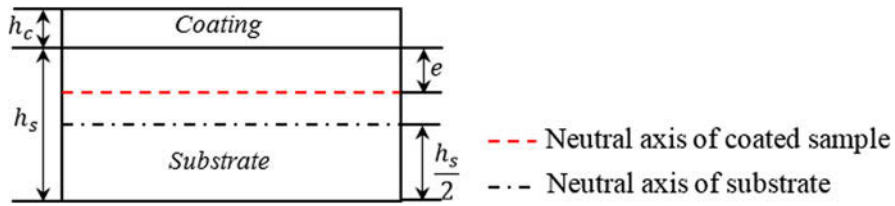


FIG. 1. Schematic representation of the shift of the neutral axis after deposition.

$$(R_f)^2 = \frac{1 + R_h^3 R_E + \frac{3R_h R_E (1 + R_h)^2}{1 + R_h R_E}}{1 + R_h R_E} \quad (18)$$

Inverting Eq. (18) leads to getting the following second degree equation which allows to determine the Young's modulus of the coating.

$$A(R_E)^2 + B(R_E) + C = 0 \quad (19)$$

Where

$$A = (R_h)^4 \quad (20)$$

$$B = 4(R_h)^3 + (6 - R_\rho R_f^2)(R_h)^2 + (4 - R_f^2)(R_h) \quad (21)$$

$$C = 1 - R_f^2(1 + R_\rho R_h) \quad (22)$$

Based on the same hypothesis of the flexural rigidity, this bilayer model has been extended analytically to a three layers model.¹⁴ It has been used to determine the Young modulus of the interface layer (E_i) between the coating and the substrate.¹⁴

$$(R_f)^2 = \frac{1 + 4R_h R_{E_i} + 4R_h R_E}{1 + R_{h_i}(R_{E_i} + R_{\rho_i}) + R_h(R_E + R_\rho)} \quad (23)$$

The indexes i and t mean the interface and the three layers beam respectively.

Where:

$$R_{h_i} = \frac{h_i}{h_s}$$

$$R_{E_i} = \frac{E_i}{E_s}$$

$$R_{\rho_i} = \frac{\rho_i}{\rho_s}$$

$$R_f = \frac{f_t}{f_s}$$

3. Berry's model

Berry's model²² is a simplified approach which can be obtained from the first order Taylor series expansion of either Pautrot's or Lopez's models.

$$(R_f)^2 = 1 + R_h[3R_E - R_\rho] \quad (24)$$

$$E_c = \frac{E_s}{3} \left[R_\rho + \frac{(R_f)^2 - 1}{R_h} \right] \quad (25)$$

B. Model based on the classical laminated beam theory (CLBT)

This model is based on the classical laminated beam theory, and allows the determination of the elasticity modulus of an individual thin film in multilayers coatings.¹² It uses the assumption that the laminated beam is symmetric, which does not correspond to the common configuration where a film is deposited only on one side of the substrate. However, the formalism can be used as an approximation for asymmetric configuration but it becomes inaccurate in the case of thick films and large R_E and R_ρ ratios. In the case of a free-free beam, the frequency of multilayers coatings can be expressed as:

$$f_t = \frac{3.561}{l^2} \sqrt{\frac{1}{d_{11} \rho_{\text{eff}}}} \quad (26)$$

The frequency ratio:

$$(R_f)^2 = 11.37 \frac{\rho_s}{d_{11} \rho_{\text{eff}} E_s} \quad (27)$$

For a one layer coating (substrate + coating):

$$d_{11} = \frac{\frac{H_1 E_s}{3(1-\nu_s^2)} + \frac{H_2 E_c}{3(1-\nu_c^2)}}{\left[\frac{H_1 E_s}{3(1-\nu_s^2)} + \frac{H_2 E_c}{3(1-\nu_c^2)} \right]^2 + \left[\frac{H_1 \nu_s E_s}{3(1-\nu_s^2)} + \frac{H_2 \nu_c E_c}{3(1-\nu_c^2)} \right]^2} \quad (28)$$

$$\begin{cases} H_1 = \frac{(h_s + h_c)^3}{4} - \frac{3(h_s + h_c)^2 h_c}{4} + \frac{3(h_s + h_c) h_c^2}{2} - h_c^3 \\ H_2 = \frac{3(h_s + h_c)^2 h_c}{4} - \frac{3(h_s + h_c) h_c^2}{2} + h_c^3 \end{cases} \quad (29)$$

$$\rho_{\text{eff}} = \rho_s h_s + \rho_c h_c \quad (30)$$

In this section we have illustrated the developed models to determine the coating Young's modulus using the vibrational method. Peraud²³ and Etienne²⁴ have respectively used Berry's and Pautrot's models to determine the Young's modulus of deposited films. Mazot¹⁴ noted that the Berry's model and Lopez's model starts to diverge for a thickness ratio of coating to substrate in the order of 0.1. The difference between the models becomes larger for higher ratios. To analyze quantitatively the differences between the models, a comparison with a finite element model, taken as a reference will be performed to assess the trueness of the method. Then, an uncertainty analysis will be done to compare the behavior of the different models with regard to their sensitivity to various uncertainty sources.

IV. EXPERIMENTS

A. Deposition

Aluminum film was deposited on a stainless steel 316L substrate by DC magnetron sputtering using a 99.99% purity aluminum target, 200 mm in diameter. The chamber was pumped down with a turbomolecular pump to less than 10^{-7} Pa before filling it with argon. The target-to-substrate distance was kept equal to 11 cm and the substrate holder was rotating to ensure a perfect thickness homogeneity of the coating. The intensity applied to the aluminum target thanks to a pulsed-DC Advanced Energy Pinnacle power supply was 2.5 A (frequency = 50 kHz; time off = 5 μ s) and the argon flow rate of 20 sccm led to a chamber pressure of 0.2 Pa. The substrate dimensions are its length $l = 70.5$ mm, its width $b = 15.68$ mm, and its thickness $h_s = 0.98$ mm. The coating has the same length and width as the substrate and a thickness $h_c = 6.712$ μ m.

B. Measurement of dimensions and density

The dimensions of the substrate were measured ten times in ten different locations. The mass of the substrate was measured using a Sartorius precision balance and its density was evaluated: $\rho_s = 7738$ kg/m³.

After deposition, the mass of the bilayer sample was measured. By using a scanning electron microscope, the thickness of the film was measured ten times in different positions. Figure 2 presenting a fractured cross sectional SEM image shows that there is no significant variation in the film thickness. The difference in mass measured before and after deposition corresponds to the film. Considering the mass and the dimensions of the film, its density was estimated: $\rho_c = 2655$ kg/m³.

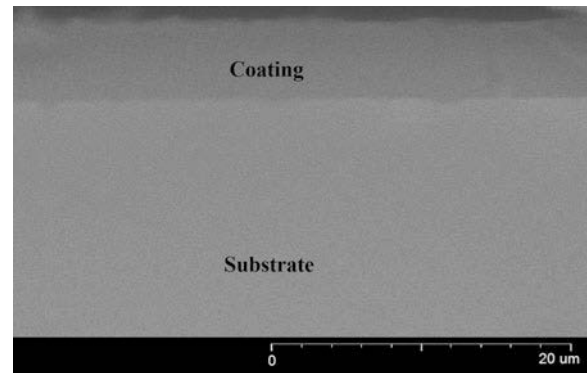


FIG. 2. Cross sectional SEM image of the aluminum film.

C. IET experimental set-up

The principle of the IET is to measure the resonance frequencies of a specimen impacted by an impulse (Fig. 3). A beam can be excited in different vibrational modes: longitudinal, flexural, and torsional.²⁰ These mechanical vibrations are detected by an acoustic microphone, and transformed by a transducer into an electrical signal which is presented as a function of time. Finally, the Fast Fourier Transform (FFT) is used to represent the signal as a function of frequency and extract the resonance frequencies of the sample. The resonance frequency, density or mass and dimensions of the sample are used to calculate the elastic constants of the material.

Before performing the test, the specimen is placed on a support (Fig. 3). The free-free boundary condition was adopted for the present procedure.²⁰ To achieve as best as possible this free-free condition, several supporting methods were used:

- (i) foam strips presenting a very low stiffness but for which the contact is large
- (ii) wires located at the nodal points of the sample where the displacement is equal to zero (for the first flexural mode used in the present study).

More detailed explanations on the procedure can be found in the literature.^{20,29} During the test some errors on the measured frequency can be introduced throughout any of the used equipment or the misplacement of the sample. These sources of error will be investigated below.

The measurement of frequencies was done with the RFDA professional signal analysis system (Resonance Frequency and Damping Analysis) from IMCE company (Genk, Belgium). It is equipped with an RFDA transducer, an automatic excitation unit, a microphone with a frequency range up to 100 kHz, a universal wire support and a computer system equipped with RFDA software (Fig. 3).

The first resonance frequency was measured before and after deposition (Fig. 4). The two measured frequencies were used to calculate the substrate Young's modulus using Eq. (4) and the film Young's modulus with the

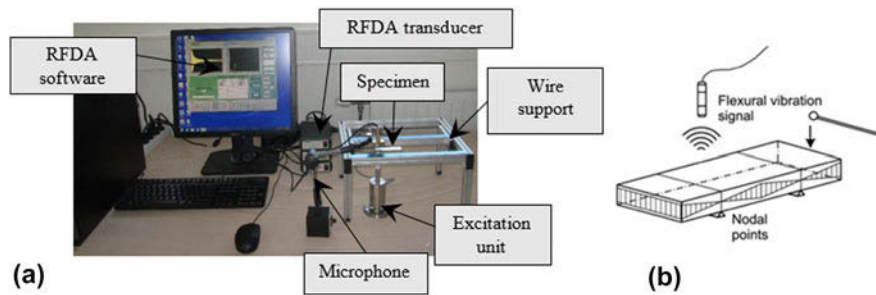
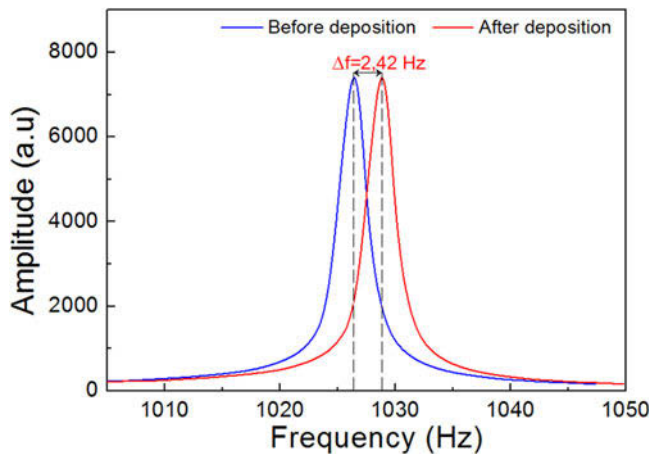
FIG. 3. (a) Experimental equipment, (b) flexural vibration mode.²¹

FIG. 4. Natural frequencies before and after deposition.

different models using Eqs. (13), (19), (25), and (27). The values of the frequencies and Young's modulus are represented in Table I.

V. NUMERICAL SIMULATION

A 3D Finite Elements Model (FEM) was developed with the commercial finite element code ABAQUS³⁰ (Fig. 5). Figure 5 represent the first vibration mode of the bilayer beam. The geometrical model is composed of two parts: the substrate and the coating. The substrate is a rectangular cross section slender beam with a length $l = 70$ mm, a width $b = 7$ mm and a thickness $h_s = 0.5$ mm. The coating was bonded on the substrate throughout the tie function³⁰ and has a thickness h_c , which was varied during analysis from 0 to 0.25 mm. Free boundary conditions were applied to the beam and the 3D stress C3D20 quadratic element was used to mesh the structure. To extract the resonance frequency of the composite beam, the ABAQUS\Implicit Lanczos eigensolver was used. A mesh convergence study was done (Fig. 6), and the element size of $(0.35 \times 0.35 \times 0.25 \text{ mm}^3)$ was chosen. This configuration is chosen as a reference to compare the analytical models proposed in the literature.

VI. TRUENESS ANALYSIS

In the metrological field, trueness is defined as the agreement of the measured value (averaged on an infinite number of measurements) and a reference value, as defined, for instance by a standard.³¹ It is associated with the notion of systematic error. In the case of the Young's modulus of thin film, the traceability to international standards is not established and no certified reference material is available. Thus it is difficult to perform a trueness study satisfactorily. However, in the present paper, two sources of systematic errors are investigated: the error linked to the model, with the FEM of Sec. V as an arbitrary reference and the error linked to the effective realization of the free-free boundary condition (which is done in Sec. VII. A. 4).

In this section a parametric comparison of the analytical models with the finite element model is done for four different R_E and R_p ratios. Figure 7 represents the evolution of the frequency ratio R_f as a function of the thickness, density, and Young's modulus ratios. We can see a very good agreement between Pautrot's model and the FEM, for any R_h , R_E , and R_p ratios. This good agreement means that, at least in the range explored in the present study, the rotatory and the shear effects are sufficiently corrected by the T_f factor of Eq. (6) in the analytical model. It is interesting to note that, in Figs. 7(c) and 7(d), the frequency variation versus R_h tends to stabilize which means that, for these configurations, the obtained modulus is not very sensitive to the film thickness.

The divergence of the other models can be clearly seen. This divergence is due to the different assumptions on which is based each model. It can be seen that the difference between the models increases with R_h ratio which was expected from the assumptions made in each model. It can be observed that the differences between the models and the reference value do not always appear in the same order. For small values of R_E and R_p , Lopez model is the closest to the Pautrot/MEF solution while, for other configurations, it is CLBT which is the closest.

A. Models systematic error study

In this work, we evaluate the systematic error of the different models taking as a reference the finite element

TABLE I. Substrate and film Young's modulus.

Frequency before deposition (Hz)	Frequency after deposition (Hz)	Substrate Young's modulus (GPa)	Film Young's modulus (GPa)			
			Lopez	Berry	Pautrot	CLBT
1026.52	1028.94	198.77	67.48	68.40	67.73	65.66

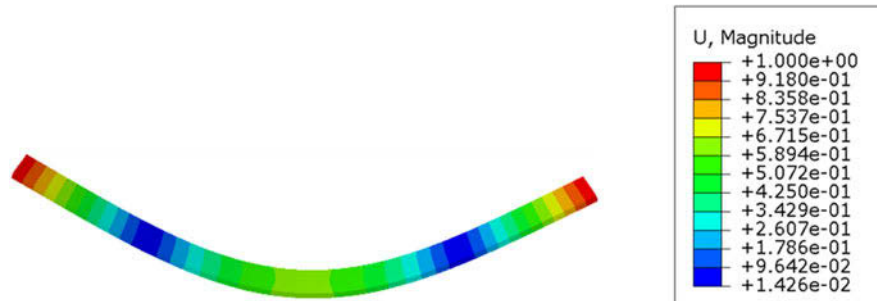


FIG. 5. Deformed beam. The colors indicate the vertical displacement (mm).

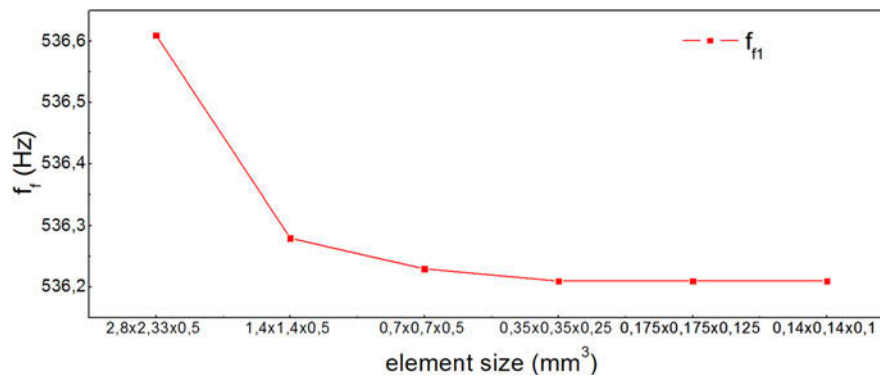


FIG. 6. Mesh convergence.

model developed in Sec. V. As mentioned in Sec. V, there is no guarantee that the FE model presents the true value.

To estimate the errors, extensive series of numerical analyses were carried out by the commercial finite element ABAQUS. The thickness ratio R_h was varied from 0.006 to 0.1, the Young's modulus ratio R_E from 0.25 to 8 and the density ratio from 0.25 to 16. The results are presented in Figs. 8–10.

Figure 8 shows the evolution of the systematic error of Lopez's model as a function of Young's modulus ratio R_E and thickness ratio R_h . The gray zone represents an error higher than 10%. It is clearly seen that the evolution of the error is proportional to the evolution of the distance e between the neutral axis before and after deposition (Figs. 1 and 11). Figure 11 represent the evolution of the normalized shift of the neutral axis $\frac{e}{h_s}$ as a function of the ratios R_E and R_h . The lower error zone, between 1 and 2%, is limited by a Young's modulus ratio equal to 1 and a thickness ratio equal to 0.02. On the other side, we found that the error of the Lopez's model does not

depend on the density ratio R_ρ (even though R_ρ appears in the expression of Lopez's model) so that we can conclude that the trueness error of the Lopez's model is related to the thickness and Young's modulus ratios.

Contrarily to Lopez's model, the error of Berry's model (Fig. 9) depends on the density ratio R_ρ , the Young's modulus ratio R_E , and the thickness ratio R_h . Figure 9 represents the evolution of the error as a function of the thickness, Young's modulus and density ratios. We can see that for higher thickness ratio the error is more important for the same Young's modulus and density ratios. It is interesting to note that there is a correlation between R_E and R_ρ on the systematic error and thus that an increase of one of the two ratio will not systematically lead to an increase of the error. For instance, for a small error will be obtained for $R_\rho = 14$ and $R_E = 4$. Using Berry's model, it is necessary to keep attention to the ratios mentioned above. Figure 9 can provide information about the error made.

Like Lopez's model, the error of the CLBT model does not depend on the density ratio R_ρ . On Fig. 10 we can see

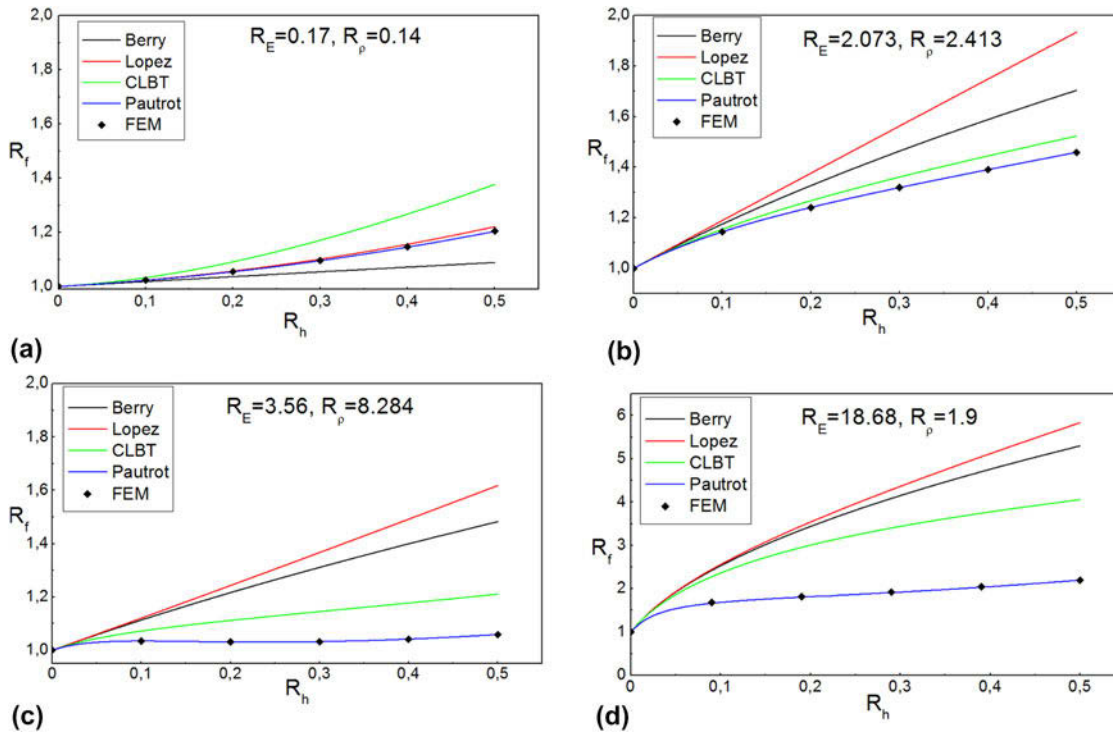


FIG. 7. Comparison between analytical and numerical models for different Young's modulus and density ratios: (a) $R_E = 0.17$, $R_p = 0.14$, (b) $R_E = 2.073$, $R_p = 2.413$, (c) $R_E = 3.56$, $R_p = 8.284$, (d) $R_E = 18.68$, $R_p = 1.9$.

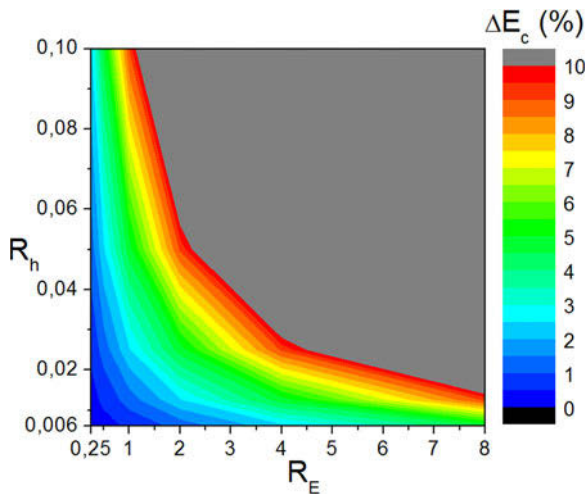


FIG. 8. Systematic error associated to Lopez's model.

the evolution of the CLBT model error as a function of the thickness and the Young's modulus ratios. We can observe that the optimum error zone is centered at a Young's modulus ratio equal to 1. This is due to the assumption of symmetry on which is based this model.

VII. UNCERTAINTY ANALYSIS

The uncertainty analysis is performed following the guidelines of current reference metrological document,

i.e., the Guide to the Expression of Uncertainty in Measurement (aka GUM), ISO 57 020 standard³² and the International Vocabulary of Metrology (aka VIM), JCGM 200:2012.³¹ The uncertainty on a quantity x is denoted $u(x)$ which represents the standard uncertainty, that is, the standard deviation of the distribution of x values, obtained either experimentally from a series of measurements either estimated from various assumptions. Not all the uncertainty sources are taken into account in the present paper. For instance the definitional uncertainty and the instrumental measurement uncertainty were neglected. The former represents the uncertainty linked to the definition of the measurand while the latter denotes the uncertainty arising from the measurement system. Here, the measurand (the measured quantity) is defined as the Young's modulus of the unique specimen, i.e., fluctuations due to the manufacturing process are neglected and its value is assumed to be homogeneous in the film or in the substrate. The elastic behavior of the film and the substrate is assumed to follow the isotropic Hooke's law, i.e., the effects of texture, for instance, are neglected. Uncertainties coming from the measurement system such as those linked to the window used for computing the FFT and the signal discretization are assumed to be negligible. It can be noted that the GUM methodology can be criticized by some experts in metrology, however its aim is to be standardized to be relatively easy to use by a non-expert in metrology.

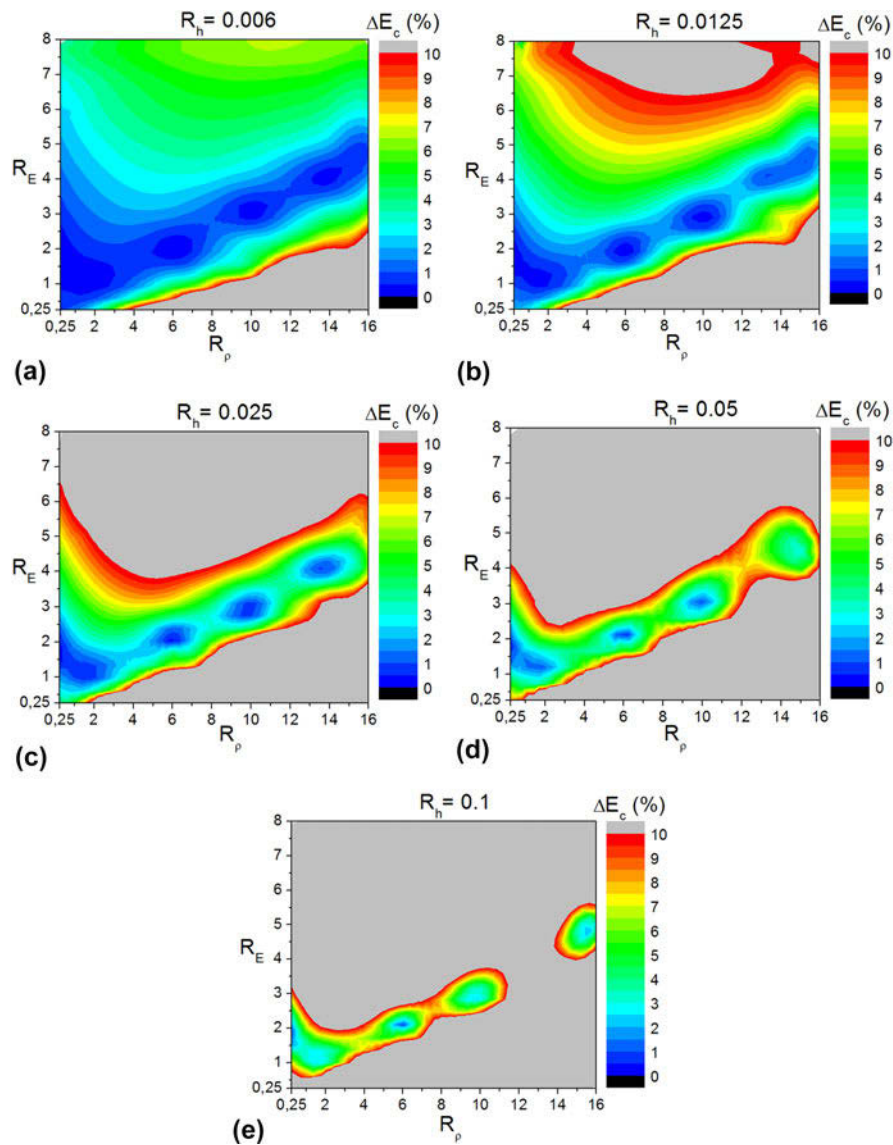


FIG. 9. Systematic error associated to Berry's model for different Young's modulus, density and thickness ratios: (a) $R_h = 0.006$, (b) $R_h = 0.0125$, (c) $R_h = 0.025$, (d) $R_h = 0.05$, (e) $R_h = 0.1$.

Some components of the uncertainty considered in the present study can be calculated using the uncertainty propagation equation, like in the study done by Bullough,³³ and some others do not appear explicitly in the models. The latter are generally linked to the measurement technique and the apparatus. In our case the frequency is investigated (repeatability and sample positioning) and its uncertainty calculated experimentally.

A. Frequency error investigations

An experimental study was done to estimate the uncertainty on the measured frequency through the different possible sources of error. In the following we will present the sources which influence significantly the frequency measurement.

1. Repeatability

The RFDA system (Fig. 3) was used to determine the first four flexural resonance frequencies of a slender steel substrate which dimensions are given in Sec. IV. A. The nylon wires support provided with the instrument was taken as a reference. To excite the desired mode, the wires of the supports were located at the respective nodal points of each mode. Each measurement was repeated thirty times, and then repeated again on a different days in the same conditions and by the same operator. The microphone was placed at a distance of 5 mm from the substrate. The angle between the nodal lines of the beam and the wires of the support is 0° . The average frequency and the repeatability uncertainty are presented in Table II. The repeatability uncertainty is calculated using Eq. (31), according to the GUM.³²

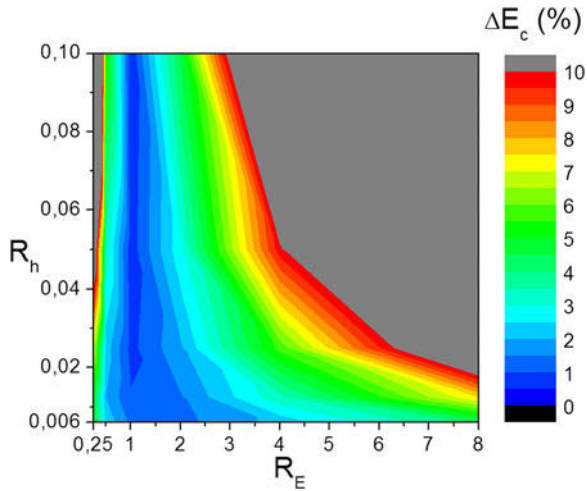
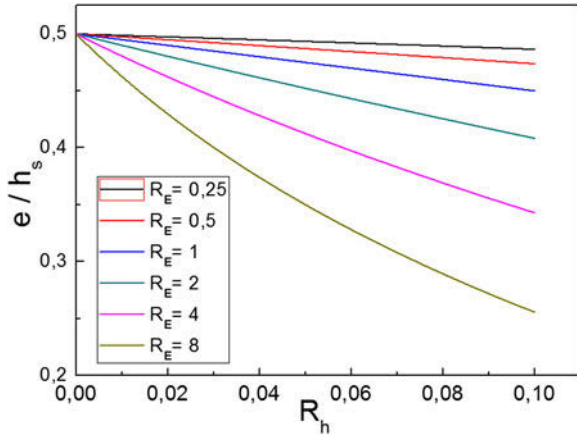


FIG. 10. Systematic error associated to CLBT's model.


FIG. 11. Evolution of the normalized shift of the neutral axis e/h_s as a function of the thickness and Young's modulus ratios.

$$u_{\text{rep}} = \frac{\sigma_{\text{exp}}}{\sqrt{j}} \quad (31)$$

Where j is the number of repeated frequency measurements and σ_{exp} is the standard deviation computed on the j measurements.

2. Position of the microphone

To study the influence of the microphone position on the frequency measurement, the microphone was placed at a distance of 5 and 10 mm from the sample. The angle between the nodal lines and the support wires was kept at 0° . The resonances frequencies measured in both configurations are presented in Table III. The difference Δf_{posit} is higher than the repeatability uncertainty, so the effect of the microphone position can be considered as significant (Tables II and III). Assuming that the error caused by the position of the microphone on the frequency

TABLE II. Repeatability uncertainty of the first four resonance frequencies.

Mode	Average frequency (Hz)	u_{rep} (Hz)
1	1032.990	0.018
2	2852.740	0.048
3	5599.100	0.077
4	9252.200	0.025

TABLE III. Effect of microphone position on the measured resonance frequencies.

Mode	Average frequency (Hz) ($d = 5$ mm)	Average frequency (Hz) ($d = 10$ mm)	Δf_{posit} (Hz)	u_{posit} (Hz)
1	1032.990	1033.054	0.064	0.018
2	2852.740	2852.880	0.140	0.040
3	5599.100	5599.180	0.080	0.023
4	9252.200	9252.660	0.460	0.133

follows a uniform distribution function between the two values obtained, the standard uncertainty can be calculated using Eq. (32)³²:

$$u_{\text{posit}} = \frac{\Delta f_{\text{posit}}}{2\sqrt{3}} \quad (32)$$

3. Misalignment between the nodal lines and the supporting wires

To study the influence of the misalignment between the nodal lines and the supporting wires on the frequency measurement, the specimen was placed on the universal support forming an angle of 5° and the microphone was placed at 5 mm from the specimen. The measured frequencies were compared with the values of Table II which correspond to 0° . The comparison is presented in Table IV. The quantity Δf_{align} is higher than the repeatability uncertainty, so the effect of misalignment is considered as significant. Like in the previous section, assuming that the error caused by the misalignment between the nodal lines and the supporting wires on the frequency follows a uniform distribution function between the two measured values, the standard uncertainty is calculated using Eq. (33)³²

$$u_{\text{align}} = \frac{\Delta f_{\text{align}}}{2\sqrt{3}} \quad (33)$$

In fact, a misalignment of 5° is easy to spot and, in practice, the corresponding uncertainty will certainly be smaller. Here, the misalignment was exaggerated to make it detectable.

4. Supports

In the models, the boundary conditions for the beam are assumed to be free-free. However, this condition is not possible in practice and different solutions can be imagined to get as close as possible to the modeling assumptions. To evaluate the influence of the nature of the support, the first four frequencies were measured by using the following supports: Nylon wire, rubber, copper wire and foam. The results are illustrated in Table V. The highest difference between the measured frequencies is higher than the repeatability uncertainty. The effect of support is thus considered as significant and the quantity Δf_{supp} is used to calculate the uncertainty u_{supp} caused by the support.

$$u_{\text{supp}} = \frac{\Delta f_{\text{supp}}}{2\sqrt{3}} \quad (34)$$

B. Uncertainty of the substrate and the film Young's moduli

Firstly we will explicit all the uncertainties which appear in Eq. (4), then the global combined standard uncertainty of the substrate Young's modulus will be calculated according to the equation of uncertainty propagation given in the GUM, assuming that the covariances between the different quantities are null³²:

$$u(E_s)^2 = \left(\frac{\partial E_s}{\partial k_1}\right)^2 u(k_1)^2 + \left(\frac{\partial E_s}{\partial k_2}\right)^2 u(k_2)^2 + \left(\frac{\partial E_s}{\partial f_s}\right)^2 u(f_s)^2 + \left(\frac{\partial E_s}{\partial \rho_s}\right)^2 u(\rho_s)^2 + \left(\frac{\partial E_s}{\partial l}\right)^2 u(l)^2 + \left(\frac{\partial E_s}{\partial h_s}\right)^2 u(h_s)^2 \quad (35)$$

1. Frequency uncertainty

The uncertainty of the first resonance frequency can be calculated by adding the square of the standard uncertainty (adding the variances) of each quantity on the measurement. In the previous section, it has been shown that the uncertainty due to the support is the most influent on the measurement.

TABLE IV. Misalignment's error.

Mode	Average frequency (Hz) ($\theta = 0^\circ$)	Average frequency (Hz) ($\theta = 5^\circ$)	Δf_{align} (Hz)	u_{align} (Hz)
1	1032.990	1033.160	0.170	0.049
2	2852.740	2853.100	0.360	0.104
3	5599.100	5599.700	0.600	0.173
4	9252.200	9252.600	0.400	0.115

$$u(f_s) = \sqrt{u_{\text{rep}}^2 + u_{\text{posit}}^2 + u_{\text{align}}^2 + u_{\text{supp}}^2} = 0.115 \text{ Hz} \quad (36)$$

Table VI shows the contribution of each uncertainty source on the uncertainty of frequency. We can see clearly that the support has the highest contribution to the global uncertainty, then the uncertainty due to the misalignment. The influence of the two other sources is small (about 5%).

2. k_1 and k_2 constants uncertainty

Supposing that the constants k_1 and k_2 were rounded, we can consider that the true value of k_1 is between 0.94645 and 0.94655 and the true value of k_2 is between 6.5845 and 6.5855. The constants uncertainty is then calculated as follows:

$$u(k_1) = \frac{0.0001}{2\sqrt{3}} = 2.810^{-5} \quad (37)$$

$$u(k_2) = \frac{0.001}{2\sqrt{3}} = 2.810^{-4} \quad (38)$$

It should be noted that these uncertainties are not physical but they are due to the finite number of digits available. The uncertainty budget shows that the influence of rounding is negligible as compared to other uncertainty sources.

3. Dimensions uncertainties

The dimensions of the substrate and the coating were measured ten times in ten different locations. The

TABLE V. Resonance frequencies of the sample placed on different supports.

Mode	Nylon wires (Hz)	Rubber (Hz)	Copper wire (Hz)	Foam (Hz)	Δf_{supp}	u_{supp}
1	1032.990	1033.200	1033.100	1033.350	0.360	0.104
2	2852.740	2852.900	2852.990	2853.030	0.290	0.084
3	5599.100	5599.660	5599.500	5599.500	0.560	0.162
4	9252.200	9252.440	9252.110	9252.250	0.330	0.095

TABLE VI. Contribution of each source error on the uncertainty of frequency.

Uncertainty source	Contribution (%)
Repeatability	2.5
Microphone position	2.6
Misalignment error	19
Support error	75.9

dimensions averages and their uncertainties are presented in Table VII. The standard uncertainties were evaluated according to a type A method by computing the standard deviation.³²

4. Density uncertainty

The uncertainties on substrate and film densities are calculated using the sample mass and dimensions. The mass uncertainty is evaluated following a type B procedure.³² According to the technical specifications of the precision balance used, the uncertainty is equal to 1 mg so the standard deviation was taken equal to $1/\sqrt{3}$ mg. The uncertainties on the substrate and the film densities are calculated as follow³²:

$$u(\rho_s)^2 = \left(\frac{\partial \rho_s}{\partial m_s}\right)^2 u(m_s)^2 + \left(\frac{\partial \rho_s}{\partial h_s}\right)^2 u(h_s)^2 + \left(\frac{\partial \rho_s}{\partial l}\right)^2 u(l)^2 + \left(\frac{\partial \rho_s}{\partial b}\right)^2 u(b)^2 \quad (39)$$

$$u(\rho_s) = 39 \text{ kg/m}^3$$

$$u(\rho_c)^2 = \left(\frac{\partial \rho_c}{\partial m_c}\right)^2 u(m_c)^2 + \left(\frac{\partial \rho_c}{\partial h_c}\right)^2 u(h_c)^2 + \left(\frac{\partial \rho_c}{\partial l}\right)^2 u(l)^2 + \left(\frac{\partial \rho_c}{\partial b}\right)^2 u(b)^2 \quad (40)$$

$$u(\rho_c) = 149 \text{ kg/m}^3$$

5. Global uncertainty

From all the uncertainties calculated in previous sections, the global uncertainty on the substrate Young's modulus was calculated using Eq. (35). The substrate Young's modulus uncertainty and the contribution of each uncertainty source are presented in Table VIII. A contribution correspond to one of the terms in Eq. (35).

From Table VIII, we can conclude that the main contribution to the global uncertainty comes from the measurement of the thickness (79%) and of the density

TABLE VII. Dimensions of the substrate and measurement uncertainty.

Dimensions	Average (mm)	Uncertainty (mm)
l	70.500	0.017
b	15.6800	0.0097
h_s	0.9800	0.0048
h_c	0.006712	0.000171

(20%). The other quantities are completely negligible. So, to increase the accuracy of Young's modulus measurement, the main efforts should be put on the accuracy of thickness.

After calculating of the uncertainty on the elasticity modulus of the substrate (Table VIII), the uncertainty of the coating Young's modulus is calculated according to the GUM, the uncertainty was calculated for all the models (Berry, Pautrot, Lopez and CLBT) to see the difference between the generated uncertainty of each model because it may happened that a more accurate model can be less stable and lead to a larger uncertainty than a simplified model, but in this case the frequency uncertainty is treated differently. The support error is now considered as systematic given that the same support will be used to measure the two frequencies before and after deposition, causing a similar shift of the two frequencies. So, to evaluate the error due to the support, it will be integrated in the different models (Pautrot, Berry, Lopez and CLBT) through the frequency ratio R_f .

$$R_f = \frac{f_t + \Delta_{\text{supp}}}{f_s + \Delta_{\text{supp}}} \quad (41)$$

Here, the error due to the support is assumed to be additive. If the error is assumed to be multiplicative, it will simplify out and lead to no error at all. Then, inverting Eqs. (13), (19), (25) and (27), the Young modulus of the film can be expressed as following:

$$E_c = E_s F(f_t, f_s, h_c, h_s, \rho_c, \rho_s, \Delta_{\text{supp}}) \quad (42)$$

Where F is a function which depends on the model used. As Δ_{supp} is smaller than 1 Hz and thus small as compared to f_s or f_t , function F can be expanded into a Taylor series and truncated to the first order. It was found that the support error represents a systematic error of about

TABLE VIII. Contribution of each uncertainty source on the substrate Young's modulus uncertainty.

Quantity		Uncertainty (GPa)	Contribution (%)
k_1		1.6×10^{-5}	7.1×10^{-4}
k_2		5.2×10^{-11}	2.4×10^{-9}
ρ_s		0.44	20.2
	Repeatability	2.2×10^{-5}	9.8×10^{-4}
	Microphone position	2.3×10^{-5}	1.0×10^{-3}
f_s	Misalignment error	1.7×10^{-4}	7.6×10^{-3}
	Support error	6.7×10^{-4}	3.0×10^{-2}
	Total for f_s	8.8×10^{-4}	0.04
l		0.017	0.76
h_s		1.7	79
	Total for E_s	2.20	100

TABLE IX. Contribution of each uncertainty source (in GPa and %) on the coating Young's modulus uncertainty.

	Pautrot		Lopez		Berry		CLBT	
	GPa	%	GPa	%	GPa	%	GPa	%
E_s	0.236	9.90	0.234	9.90	0.237	9.90	0.236	9.90
ρ_c	0.676	28.39	0.670	28.33	0.669	28.34	0.674	28.33
ρ_s	0.0052	0.22	0.0051	0.22	0.0052	0.22	0.0052	0.22
Repeatability	0.048	2.01	0.047	2.01	0.048	2.02	0.048	2.01
Microphone position	0.050	2.12	0.050	2.12	0.051	2.12	0.050	2.12
f_t Misalignment error	0.368	15.51	0.365	15.48	0.370	15.49	0.3663	15.51
Total for f_t	0.467	19.64	0.463	19.61	0.469	19.62	0.464	19.65
Repeatability	0.048	2.03	0.048	2.02	0.048	2.02	0.048	2.02
Microphone position	0.051	2.13	0.050	2.13	0.051	2.13	0.051	2.13
f_s Misalignment error	0.371	15.58	0.367	15.55	0.371	15.55	0.370	15.56
Total for f_s	0.470	19.74	0.465	19.70	0.470	19.70	0.469	19.71
h_c	0.505	21.20	0.503	21.31	0.509	21.30	0.505	21.20
h_s	0.022	0.91	0.022	0.91	0.022	0.92	0.022	0.90
Total for E_c	2.38	100	2.36	100	2.39	100	2.38	100

$5 \times 10^{-3}\%$. Based on this value, in the present case, the support error will be neglected in the calculation of uncertainty on the coating Young's modulus, but will be kept in the uncertainty on the substrate Young's modulus. This approach simplifies significantly the calculation of the uncertainty. Indeed, if the propagation of uncertainty was performed directly on Eq. (42) without the simplification, some correlations (covariances) would appear and become delicate to treat.

The uncertainty values and the contribution of each uncertainty source on the uncertainty of the coating Young's modulus are represented in Table IX.

In our case the uncertainty is in the order of 2.4 GPa (Table IX) which represents 3.5% of the measured Young's modulus. From Table IX, we can conclude that for all the models, the measure of the density and the thickness of the film, representing respectively a percentage contribution about 28% and 21% are the first to be improved. Contrarily to the case of the substrate, the uncertainty on the frequency has a significant effect on the measurement and increases from 0.04% to 19%. This is related to the small difference between the frequencies measured before and after deposition. More attention on the alignment of the nodal points of the sample with the support can give a higher precision on the measured value. It can be noted that no difference was observed on the uncertainty of the different models, nor on the magnitude of the different sources. This means that it is always better to use the more complete model. This is not always the case in inverse methods.

VIII. CONCLUSION

The Young's modulus of coatings and substrates was measured by the Impulse Excitation Technique (IET).

The elasticity modulus of the coating was obtained by different models available in the literature: Berry, Lopez, Pautrot and Classical Laminated Beam Theory. A numerical finite element model was developed and used to estimate the systematic errors given by the four analytical models. A detailed uncertainty budget was performed for each model according to the recommendation of the ISO Guide on the Expression of Uncertainty on Measurement. The following results were obtained:

(1) The reliability of Berry's model depends on the thickness, density and Young's modulus ratios and not only on the thickness ratio.

(2) Both Lopez and CLBT models depend on the thickness and Young's modulus ratios. Increasing these ratios increases the error.

(3) Pautrot's model is the most complete and it presents an almost perfect agreement with the numerical values obtained by finite elements. It is thus recommended to determine the Young's modulus of a film for any thickness, Young's modulus and density ratios.

(4) The standard uncertainty on the substrate Young's modulus is about 2.2 GPa and it is about 2.4 for the coating which, in the case of the studied material, represents about 3.5% of the measured value.

(5) The standard uncertainty on the substrate Young's modulus comes mainly from the uncertainty on its density and on its thickness. For the coating itself, the main sources of uncertainty are the density and the thickness of the coating and the frequency before and after coating. The 4 models used to calculate the Young's modulus give the same total uncertainty and the same weight of all the sources.

NOMENCLATURE

b : Width	$U(x,t)$: Displacement of a point as a function of its position (x) and time (t)
d_{11} : The (1,1) element of the bending matrix of a laminated composite	U : Uncertainty
dS: Elementary section area	u_{align} : Misalignment uncertainty
E : Young's modulus	u_{pos} : Microphone position uncertainty
e : Shift of the neutral axis after deposition	u_{rep} : Repeatability uncertainty
f : The first resonance frequency	u_{supp} : Support uncertainty
f_n : flexural resonance frequency of the n^{th} mode of vibration	X_n : Nondimensional eigenfrequencies
h : Thickness	ν_c : Coating Poisson's ratio
I : Second moment of the section	ν_s : Substrate Poisson's ratio
j : Number of repeated measurement	Δf_{align} : Misalignment error
l : Length	Δf_{posit} : Microphone position error
n : Mode of vibration	Δf_{supp} : Support error
R_E : Young's modulus ratio	ρ : Density
R_f : Frequency ratio	ρ_{eff} : Effective density
R_h : Thickness ratio	σ_c : Stress in the coating
R_ρ : Density ratio	σ_{exp} : The experimental standard deviation
S : Section area	σ_s : Stress in the substrate

ACKNOWLEDGMENTS

The authors would like to thank Région Champagne-Ardenne and Accompagnement Economique du Laboratoire de Bure-Saudron for the financial support.

REFERENCES

- C. Lopes, M. Vieira, J. Borges, J. Fernandes, M.S. Rodrigues, E. Alves, N.P. Barradas, M. Apreutesei, P. Steyer, C.J. Tavares, L. Cunha, and F. Vaz: Multifunctional Ti–Me (Me = Al, Cu) thin film systems for biomedical sensing devices. *Vacuum* **122**, 353–359 (2015).
- A.S.H. Makhlof: Protective coatings for automotive, aerospace and military applications: Current prospects and future trends. In *Handbook of Smart Coatings for Materials Protection*, A.S.H. Makhlof, ed. (Woodhead Publishing, Cambridge, 2014); pp. 121–131.
- J.G. Tait, B.J. Worfolk, S.A. Maloney, T.C. Hauger, A.L. Elias, J.M. Buriak, and K.D. Harris: Spray coated high-conductivity PEDOT:PSS transparent electrodes for stretchable and mechanically-robust organic solar cells. *Sol. Energy Mater. Sol. Cells* **110**, 98–106 (2013).
- A. Billard and F. Perry: Pulvérisation cathodique magnétron. *Techniques de l'Ingénieur*, M1654 (2005).
- J.A. Thornton: Influence of apparatus geometry and deposition conditions on the structure and topography of thick sputtered coatings. *J. Vac. Sci. Technol.* **11**, 666–670 (1974).
- C. Bellan and J. Dhers: Evaluation of Young modulus of CVD coatings by different techniques. *Thin Solid Films* **469–470**, 214–220 (2004).
- M. Radovic, E. Lara-Curzio, and L. Rierster: Comparison of different experimental techniques for determination of elastic properties of solids. *Mater. Sci. Eng., A* **368**, 56–70 (2004).
- Y. Tan, A. Shyam, W.B. Choi, E. Lara-Curzio, and S. Sampath: Anisotropic elastic properties of thermal spray coatings determined via resonant ultrasound spectroscopy. *Acta Mater.* **58**, 5305–5315 (2010).
- P. Sedmák, H. Seiner, P. Sedlák, M. Landa, R. Mušálek, and J. Matějček: Application of resonant ultrasound spectroscopy to determine elastic constants of plasma-sprayed coatings with high internal friction. *Surf. Coat. Technol.* **232**, 747–757 (2013).
- M. Thomasová, P. Sedlák, H. Seiner, M. Janovská, M. Kabla, D. Shilo, and M. Landa: Young's moduli of sputter-deposited NiTi films determined by resonant ultrasound spectroscopy: Austenite, R-phase, and martensite. *Scr. Mater.* **101**, 24–27 (2015).
- P. Gadaud and S. Pautrot: Application of the dynamical flexural resonance technique to industrial materials characterisation. *Mater. Sci. Eng., A* **370**, 422–426 (2004).
- A. López-Puerto and A.I. Oliva: A vibrational approach to determine the elastic modulus of individual thin films in multilayers. *Thin Solid Films* **565**, 228–236 (2014).
- P. Gadaud, X. Milhet, and S. Pautrot: Bulk and coated materials shear modulus determination by means of torsional resonant method. *Mater. Sci. Eng., A* **521–522**, 303–306 (2009).
- P. Mazot and S. Pautrot: Détermination du module d'young de dépôts par flexion dynamique: Application aux systèmes bicouche et tricouche. *Ann. Chim. Sci. Mat.* **23**, 821–827 (1998).
- G. Pickett: Equations for computing elastic constants from flexural and torsional resonant frequencies of vibration of prisms and cylinders. *Am. Soc. Test. Mater., Proc.* **45**, 846–865 (1945).
- W.E. Tefft: Numerical solution of the frequency equations for the flexural vibration of cylindrical rods. *J. Res. Natl. Bur. Stand., Sect. B* **64B**, 237–242 (1960).
- S. Spinner, T.W. Reichard, and W.E. Tefft: A comparison of experimental and theoretical relations between Young's modulus and the flexural and longitudinal resonance frequencies of uniform bars. *J. Res. Natl. Bur. Stand., Sect. A* **64A**, 147–155 (1960).
- S. Spinner and R.C. Valore: Comparison of theoretical and empirical relations between the shear modulus and torsional resonance frequencies for bars of rectangular cross section. *J. Res. Natl. Bur. Stand.* **60**, 459–464 (1958).
- W.E. Tefft and S. Spinner: Torsional resonance vibrations of uniform bars of square cross section. *J. Res. Natl. Bur. Stand., Sect. A* **65A**, 167–171 (1961).
- ASTM E1876–15: Standard test method for dynamic Young's modulus, shear modulus, and Poisson's ratio by impulse excitation of vibration (2015).
- R.R. Atri, K.S. Ravichandran, and S.K. Jha: Elastic properties of in-situ processed Ti–TiB composites measured by impulse excitation of vibration. *Mater. Sci. Eng., A* **271**, 150–159 (1999).
- B.S. Berry and W.C. Pritchett: Vibrating reed internal friction apparatus for films and foils. *IBM J. Res. Dev.* **19**, 334–343 (1975).

23. S. Peraud, S. Pautrot, P. Villechaise, P. Mazot, and J. Mendez: Determination of Young's modulus by a resonant technique applied to two dynamically ion mixed thin films. *Thin Solid Films* **292**, 55–60 (1997).
24. S. Etienne, Z. Ayadi, M. Nivoit, and J. Montagnon: Elastic modulus determination of a thin layer. *Mater. Sci. Eng., A* **370**, 181–185 (2004).
25. S.S. Rao: *Vibration of Continuous Systems* (John Wiley & Sons, Inc., Hoboken, 2006).
26. L. Pagnotta and G. Stigliano: Elastic characterization of isotropic plates of any shape via dynamic tests: Practical aspects and experimental applications. *Mech. Res. Commun.* **36**, 54–161 (2009).
27. J. Gere: *Mechanics of Materials* (Cengage Learning, Independence, 2003).
28. D. François: *Essais mécaniques et lois de comportement* (Éditions Lavoisier, Cachan, 2001).
29. J.D. Lord and R. Morrell: *Measurement Good Practice Guide No. 98, Elastic Modulus Measurement* (National Physical Laboratory, Middlesex, UK, 2007).
30. Abaqus Analysis User's Manual (6.12).
31. JCGM 200:2012: International vocabulary of metrology—Basic and general concepts and associated terms (VIM) (2012).
32. JCGM 100:2008(E): Evaluation of measurement data—Guide to the expression of uncertainty in measurement (2008).
33. C.K. Bullough: The determination of uncertainties in Dynamic Young's Modulus. Standards Measurement & Testing Project No. SMT4-CT97-2165 (2000).